PHYSICAL REVIEW B **86**, 054116 (2012)

Investigation of nickel lattice sites in diamond: Density functional theory and x-ray absorption near-edge structure experiments

Etienne Gheeraert,[*] Amit Kumar,[†] Etienne Bustarret, Laurent Ranno, Laurence Magaud, and Yves Joly
Institut Néel, CNRS and Université Joseph Fourier, 25 rue des Martyrs, BP166, 38042 Grenoble Cedex 9, France

Sakura Pascarelli and Matthew Ruffoni
European Synchrotron Radiation Facility (ESRF), Boîte Postale 220, F-38043 Grenoble Cedex, France

Devesh Kumar Avasthi
Materials Science Group, Inter-University Accelerator Centre, New Delhi 110067, India

Hisao Kanda[‡]
National Institute for Materials Science, 1-1 Namiki, 305-0044 Tsukuba, Japan

(Received 4 May 2012; revised manuscript received 30 July 2012; published 22 August 2012)

Possible lattice incorporation sites for Ni in diamond have been investigated using *ab initio* density functional theoretical calculations. The results have been used to compute x-ray absorption near-edge structure spectra which were compared to spectroscopic measurements performed on a diamond single crystal grown at high pressure and high temperature in a nickel solvent. Ni at divacancy sites is proposed to be the most stable and probable configuration in this crystal.

DOI: 10.1103/PhysRevB.86.054116 PACS number(s): 61.72.Bb, 61.72.up, 61.72.Dd, 71.15.Nc

I. INTRODUCTION

Besides purely academic issues, interest in the so-called color centers of diamond, nurtured for decades by esthetical and economical gemnology-related stakes, has recently been renewed by the possible application of such centers to quantum information processing. The weak coupling of impurities with lattice phonons of this transparent crystal, combined with its high thermal conductivity, leads to defects which may be investigated at an individual level[1] and can act as highly photostable single photon sources operating at room temperature. The most striking example is the nitrogen-vacancy (NV) center which has been used as both an electrically controllable single photon source[2] and a nanoscale magnetometer,[3,4] but other impurities such as Si[5,6] or transition metals[7–12] are also currently investigated for their optical emission quantum properties. Ion implantation has been quite popular in this context,[12,13] but a few impurities may also be incorporated within the dense diamond crystal during chemical vapor deposition or high pressure and high temperature (HPHT) growth without clustering: on substitutional sites, B (electron acceptor), P (donor), N, and Si; and as intersitials, H, He, and Li. To our knowledge, the only transition metals in this category are Co[8] and Ni.[7,14] Co has been tentatively suggested as a dopant in diamond seen as a new diluted magnetic semiconductor for spintronics.[15–17] Ni in diamond has been frequently proposed as a single photon source for quantum cryptography,[10–13,18] as well as a deep trap for radiation dosimetry[19,20] or a pulsed magnetic field calibration probe.[21] Contrary to B, P, and N for which extensive physicochemical data are available, equivalent experimental knowledge about Co- or Ni-doped diamond is severely lacking. One of the objectives of the present x-ray absorption near-edge structure (XANES) study at the K edge of Ni is to partially bridge this gap.

Over the last two decades, several theoretical approaches have been applied to Ni-related defects in diamond, using first small cluster calculations where atomic relaxation processes were not described properly.[22–27] The subject was then revisited employing *ab initio* density functional theory (DFT) calculations with periodic boundary conditions,[28–30] providing additional insight into the microscopic structure of various Ni-related centers in diamond. A general conclusion of the more recent studies is that isolated Ni atoms, either substitutional or at one of the interstitial sites, are not so stable and that complexes of one Ni atom with vacancies or other chemical impurities are more likely to occur under equilibrium conditions. However, not all open issues have been settled. In this work we not only calculate by *ab initio* methods the energy and stability of the Ni lattice sites but also compare quantitatively the experimental data to the simulated XANES response computed for each relaxed site.

From an experimental point of view, the various lines detected by electronic paramagnetic resonance (EPR)[31–36] or by magneto-optical (including magnetic circular dichroism) or piezo-optical spectroscopy[21,37–39] have been attributed to specific incorporation sites of Ni in diamond. This has been a challenge since the early days when it was recognized that an isolated Ni atom was incorporated in a site of trigonal symmetry at low temperatures (below 25 K) changing over to a tetrahedral symmetry at higher temperatures. Twenty years later, despite the efforts of both experimentalists and theoreticians, the identification of Ni lattice sites in diamond remains controversial.[30,35] Our contribution to this debate is based on the characterization of one nickel-doped diamond crystal by cathodoluminescence, magnetometry, and XANES presented in Sec. III, on the DFT calculations reported in Sec. IV, and on the theoretical XANES spectra described in Sec. V. The microscopic nature of the Ni lattice sites in this sample are discussed in Sec. VI. In this section, before concluding, we also tentatively relate the present analysis to the results of a thorough magneto-optical study performed recently at high fields and low temperatures on the same diamond crystal.[39]

©2012 American Physical Society

II. TECHNICAL DETAILS

The diamond crystal studied was grown in pure nickel solvent under HPHT conditions and has a yellow color without any visible inclusion. Because no nitrogen getter was added to the solvent, a significant nitrogen contamination occurred in the crystal. The type Ib diamond seed crystal was removed before characterization. According to secondary ion mass spectroscopy measurements, performed on a different sample grown under similar conditions, the nickel concentration is expected to be around 10^{19} cm^{-3}, and the nitrogen concentration is expected to be about the same. Note that due to the dependence of the impurity incorporation rate on the crystallographic orientation during growth, the impurity concentration varies depending on the growth sector. The crystal was characterized by cathodoluminescence at 5 K with a 30-kV electron beam. Magnetic properties were measured using a superconducting quantum interference device (SQUID) from 2 K to 300 K. X-ray absorption near edge structure (XANES) experiments are performed at the beam line BM29 at the European Synchrotron Radiation Facility, Grenoble. Spectra were measured at the Ni K edge ($E_0 = 8.3$ keV) in fluorescence mode, using a Ge solid state detector oriented at 45° with respect to x-ray propagation direction.

The structure and electronic properties of nickel and nickel-nitrogen complexes were investigated using the Vienna Ab-initio Simulation Package (VASP) code.[40] It is based on density functional theory (DFT) within the generalized gradient approximation.[41] A projector augmented wave was used with a basis cutoff equal to 368 eV.[42] The Monkhorst-Pack scheme[43] was used for integration in the Brillouin zone on a $5 \times 5 \times 5$ k-point mesh. The calculations were performed in a $3 \times 3 \times 3$ cubic cell (216 atoms). After convergence, residual forces were lower than 0.012 eV/Å. The calculation of the energy band gap for pure diamond ($E_g = 4.2$ eV) is in good agreement with theoretical calculations.[44,45] Total energies come out of the calculations but a direct comparison is not possible when the complexes involve different numbers of atoms of different kinds. To do so, we calculated the grand potential $\Omega(X)$ for the different complexes X in a neutral charge state:

$$\Omega(X) = E(X) - \sum_i \mu_i n_i, \tag{1}$$

where $E(X)$ is the total energy of the supercell that models complex X, n_i is the number of atoms of species i, and μ_i is their chemical potential. The chemical potential of carbon atoms was deduced from the total energy of a $3 \times 3 \times 3$ diamond cell, $\mu_C = E(\text{diamond})/216$. We made no assumption for the chemical potentials of Ni and N. As a consequence, we can compare the total energies of Ni centers that involve different numbers of C atoms as long as the relative numbers of Ni and N atoms remain the same. For each class of complex (class 1, C atoms + Ni atoms; class 2, C atoms + 1Ni + 1N; class 3, C atoms + 1Ni + 2N), we calculated corrected energies according to Eq. (1). This corrected energy is the one to be used to discuss relative stability.

Experimental XANES spectra were simulated using the FDMNES code.[46] This code is also *ab initio* DFT but uses the multiple scattering theory (MST) in a cluster approach, well adapted for the photoelectron energy range. It has been checked that working with the finite difference method, allowing a more precise description of the potential, did not improved the results. The x-ray absorption spectra were calculated for all the possible sites listed in Table I. As input we used the relaxed atomic positions obtained by the DFT

TABLE I. Summary of total energy and magnetic moment of Ni defects in a diamond matrix. The corrected energy is the energy calculated using Eq. (1) for a common reference.

Lattice site	Name	Cluster composition	Total energy (eV)	Corrected energy (eV)	Magnetic moment (μ_B)
Diamond	Diamond	216 C	−1961.24	0	0.0
Class 1: 1Ni	Corrected energies per Ni atom				
Ni$_S$	Substitutional	215C + 1Ni	−1950.358	1.799	1.97
Ni$_T$	Tetrahedral interstitial	216C + 1Ni	−1952.740	8.5	0.2
Ni$_H$	Hexagonal interstitial	216C + 1Ni	−1952.399	8.837	0.2
Ni$_S$Ni$_S$	Ni pair[a]	214C + 2Ni	−1941.67		
Ni$_S$-Ni$_S$	Two distant Ni[b]	214C + 2Ni	−1938.95		3.97
VNi$_I$V	Ni$_I$ divacancy	214C + 1Ni	−1942.977	0.1	2.14
Class 2: 1Ni,1N	Corrected energies per (Ni,N) pair				
Ni$_S$N$_S$	Ni-N complex	214C + 1Ni + 1N	−1949.619	−6.54	1.0
Ni$_T$N$_S$	Ni-N complex	215C + 1Ni + 1N	−1949.81	2.35	
Ni$_S$N$_T$	Ni-N complex	215C + 1Ni + 1N	−1947.35	4.81	
N$_S$VNi$_I$V	Ni divacancy + 1N	213C + 1Ni + 1N	−1943.283	−9.29	1.03
Class 3: 1Ni,2N	Corrected energies for 1Ni and 2N				
N$_S$N$_S$VNi$_i$V	Ni divacancy + 2N	212C + 1Ni + 2N	−1943.214	−18.30	0
N$_S$VNi$_I$VN$_S$	Ni divacancy + 2N[c]	212C + 1Ni + 2N	−1942.546	−17.63	0
N$_S$VNi$_I$VN$_S$	Ni divacancy + 2N[d]	212C + 1Ni + 2N	−1943.034	−18.12	0

[a] Two substitutional Ni atoms as first neighbor (separation distance $a\frac{\sqrt{3}}{4}$, a being the diamond lattice constant).

[b] Two substitutional Ni atoms separated by one lattice constant a.

[c] One N atom on each side of an Ni atom with inversion symmetry.

[d] One N atom on each side of an Ni atom without inversion symmetry.

calculation. We also used the nonrelaxed ones for comparison. Convergence versus the radius of the cluster around the absorbing atom was checked. At 5 Å (that is, with an 85-atom cluster), it is already satisfactory. The first series of simulations was thus performed using this radius in order to select the best Ni site. When this one was found, further refinements were performed with a 7-Å radius, that is, with around 255 atoms in the cluster.

III. DIAMOND CRYSTAL CHARACTERIZATION

The diamond crystal was first characterized by cathodoluminescence. The spectrum (Fig. 1) recorded on growth sector (111), reveals mainly the so-called 1.4-eV nickel center. The high spectral resolution spectrum reveals two peaks of similar intensities located at 1.401 and 1.404 eV. Careful optical studies of the fine structure attributed unambiguously this center to a defect containing one single nickel atom,[47] the intensities of the lines observed in the fine structure being related to the natural abundances of nickel isotopes. This optical feature has been unambiguously associated with the EPR center NIRIM-2,[47] but has a controversial origin. It has been attributed to isolated interstitial nickel Ni$_i^+$,[29] VNi$_i^+$ (3d^9) in a NiB complex,[35] and recently to the nickel divacancy VNi$_i^+$V (Ref. 36) (also called double semivacancy if Ni is considered in a substitutional site). Besides this dominant feature, the nickel-related 2.56-eV center and two nitrogen-related complexes, at 2.463 and 2.156 eV, appear on growth sector (111). Note that the incorporation of nickel depends on the concentration of nitrogen. The 1.4-eV center is observed only in diamond crystals with low nitrogen concentration, typically below 5×10^{19} cm^{-3}. For nitrogen-rich crystals ([N] $\gg$ [Ni]), the 1.4-eV center is weak and other optical structures such as 1.883 and 2.51 eV are dominant.[48] The main incorporation site of nickel is therefore expected to be the one associated with the 1.4-eV center as the nitrogen concentrate is low in the crystal studied, and the absence of the 793.6-nm line confirms that nitrogen impurities are not in aggregates.[49]

Magnetometry measurements show at 300 K the diamagnetic component of the diamond crystal and at 4 K a paramagnetic contribution of the crystal (Fig. 2). Assuming a magnetic moment of 2 μ_B per magnetic center (μ_B being the Bohr magneton), as it would be for Ni$_S$ and VNi$_I$V centers according to DFT calculations (see below), a concentration of 1.5×10^{19} cm^{-3} centers was deduced. Such a Ni incorporation corresponds to a relative concentration of 80 ppm; i.e., the Ni-Ni average first neighbor distance corresponds to 25 carbon atoms. In such a highly diluted magnetic system, weak interactions between magnetic ions and paramagnetic behavior are expected. This value being of the same order of magnitude as the nickel concentration, we conclude that a significant part of the nickel atoms are incorporated in noninteracting isolated magnetic centers. In particular, there is no significant nickel clustering in this crystal that would have induced a ferromagnetic component of the crystal magnetic moment. The Ni K edge x-ray absorption spectrum of the diamond crystal is shown in Fig. 3, with the absorption edge appearing at 8.33 keV, corresponding to electronic transitions from the 1s core level. Near-edge structures, or XANES, induced by interference between the x-ray photoelectron and the local potential fluctuations, reveal the local environment of Ni. Higher energy fine structures, or EXAFS, are not exploitable because of poor signal to noise ratio. As a first comparison,

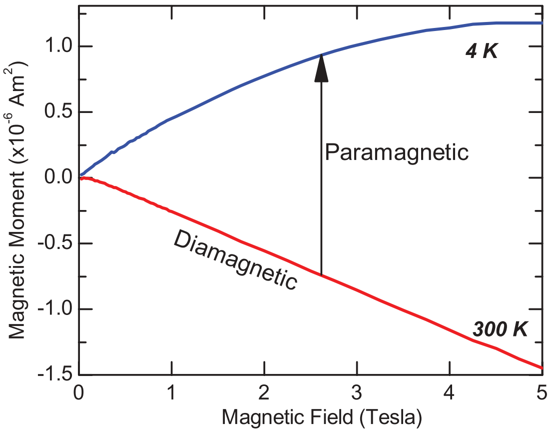

FIG. 2. (Color online) Magnetization of the Ni-doped diamond crystal recorded at 4 and 300 K. The crystal has a diamagnetic behavior at 300 K, with negative susceptibility, and paramagnetic behavior at 4 K.

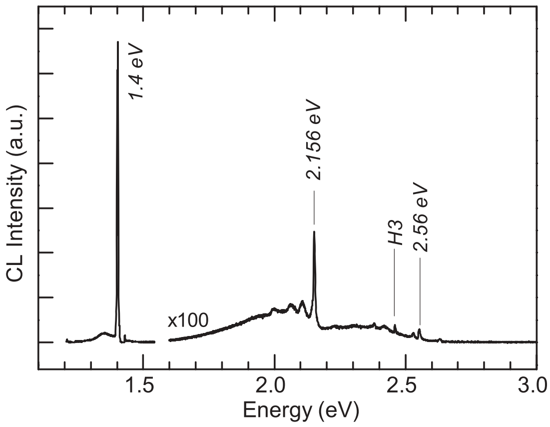

FIG. 1. Cathodoluminescence spectrum recorded at 5 K on the (111) growth sectors of the nickel-doped diamond crystal.

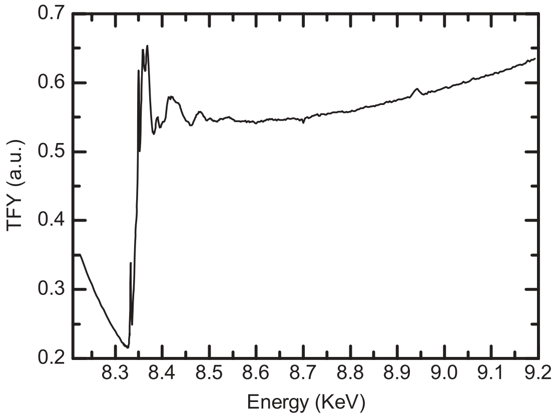

FIG. 3. XANES spectrum of the Ni-doped diamond crystal recorded near the Ni K absorption edge.

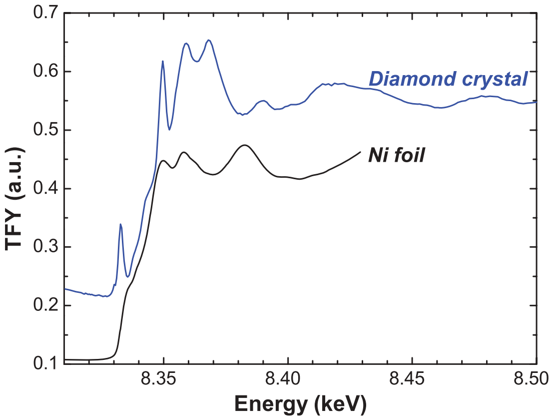

FIG. 4. (Color online) X-ray absorption of the Ni-doped diamond crystal compared to the one on a nickel foil.

a XANES signal of a nickel foil recorded in transmission is also plotted in Fig. 4. If the threshold appears at the same energy, the detailed fine structure indicates that the lattice site of Ni in diamond is obviously different from that in bulk nickel.

IV. DFT CALCULATIONS

The most probable Ni lattice sites in diamond were analyzed by DFT calculations. Results are gathered in Table I. We determined total energies, relaxed atomic positions, and magnetic moments for different classes of defects: the first category only involves Ni atoms; the second class one Ni atom and one N atom; and in the third class, the N density is twice the Ni density. We start with the first class of defects. The substitutional site (S) is obtained by replacing one C atom by one Ni atom, as shown in Fig. 5. The tetrahedral (T) interstitial site lies equidistant from four carbon atoms and the hexagonal (H) interstitial site lies midway between two T sites. In this first case, we correct the calculated total energy of the different cells by subtracting the number of C atoms times μ_C and dividing by the number of Ni atoms. As already pointed by Goss *et al.*,[28] the substitutional site is the most stable configuration within these three complexes. The Ni_S atom carries a magnetic moment equal to 1.97 μ_B. H and T sites have much smaller magnetic moments ($\mu = 0.2\ \mu_B$). The Ni_S relaxed atomic position is shown in Fig. 5. The Ni atom induces an outward relaxation of the adjacent carbon atoms. This occurs because the radius of Ni is 57% larger than that of carbon. The Ni-C first nearest-neighbor distance is equal to 1.77 Å (C-C equal to 1.54 Å in diamond). To mimic Ni segregation, we then modeled substitutional Ni pairs in the first neighbor sites separated by a diamond lattice vector. As shown in Table I the first neighbor Ni pair is the most stable one.

Finally, other low energy sites for transition metals in silicon[50] and diamond[34,51] have been proposed, in particular, the double semivacancy $V_{1/2}\mathrm{Ni}_S V_{1/2}$, also called divacancy VNiV. A divacancy site is created by removing two neighboring C atoms and placing one Ni at their midpoint, as shown in Fig. 5 in relaxed position. Among all the lattice sites that only involve Ni atoms, the Ni divacancy is the energetically most favorable configuration. The Ni atom carrying a magnetic moment equal to 2.1 μ_B.

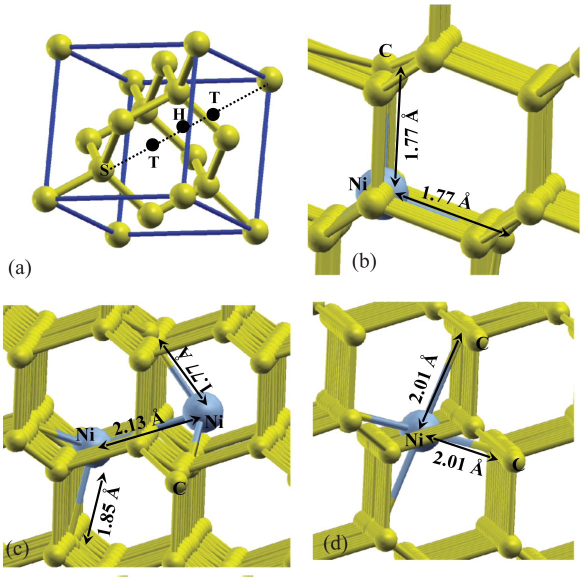

FIG. 5. (Color online) (a) Schematic of the possible sites for foreign atoms in diamond cell. The substitutional site (S) replacing one carbon atom by foreign atoms. The tetrahedral (T) sites lie equidistant from four carbon atoms and the hexagonal (H) site lies midway between two T sites. Completely relaxed structure of a Ni atom at (b) substitutional Ni_S, (c) two nearest-neighbor Ni_S atoms, and (d) Ni divacancy ($\mathrm{VNi}_I\mathrm{V}$). The carbon atoms are shown as golden circles and the nickel atoms are shown as blue circles.

In order to understand the effect of nitrogen on the incorporation of nickel, Ni-N complexes have been studied in the following configurations (corresponding to the second group of complexes) (Fig. 6):

(a) (Ni_S-N_S) complex, both nickel and nitrogen atoms at the substitutional sites;

(b) (N_S-Ni_T) complex, nitrogen atom at the substitutional site and Ni atom at the tetrahedral site;

(c) (Ni_S-N_T) complex, nickel atom at the substitutional site and nitrogen atom at the tetrahedral site; and

(d) ($\mathrm{VNi}_I\mathrm{V} + \mathrm{N}_S$) complex, Ni divacancy plus one N atom.

The corrected energies of Table I are expressed for one (Ni,N) pair.

In the case of the Ni-N complex, (Ni_S-N_S) is the most stable configuration of the three first complexes but the nitrogen-decorated nickel divacancy where one C first neighbor is replaced by one N atom is even more stable. When nickel and nitrogen atoms lie at substitutional sites the Ni-N bond length is 1.78 Å.

The last class of calculated defects involves a divacancy decorated by two N atoms (Fig. 7). Three configurations are possible: in the first one, the two N atoms are on the same side of the Ni atom. In the second and third configurations they are situated on both sides of the Ni atom with an inversion symmetry in the second case and none in the third. The case with two N atoms on the same side corresponds to the lowest energy.

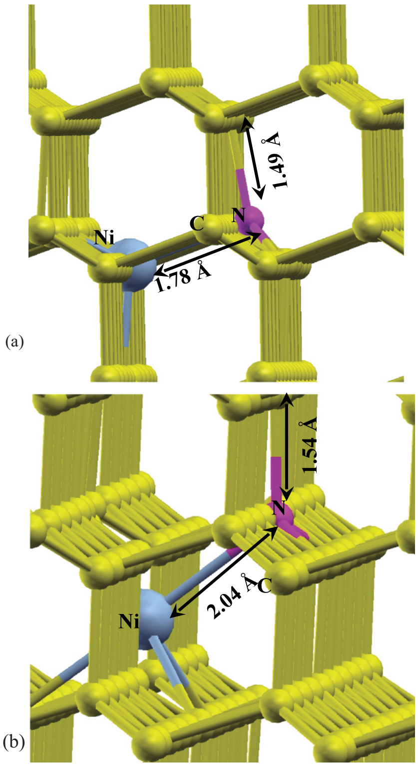

FIG. 6. (Color online) Relaxed structure of two configurations of the Ni-N complex: (a) (Ni_S-N_S) complex, both nickel and nitrogen atoms at substitutional sites, and (b) Ni divacancy decorated with one substitutional nitrogen atom (VNi_IVN_S)

V. XANES CALCULATIONS

Figure 8 shows the XANES simulated spectra corresponding to the substitutional site (S), the hexagonal interstitial site (H), and the tetrahedral interstitial site (T) for the Ni atom in diamond. When comparing with the experimental spectra, the S site could appear as the best because all the main features are present. Nevertheless their relative intensity is not well suited. The T site is definitely inadequate and can be rejected. The H site shows the double bump at 8.36–8.37 keV but reveals also extra features on the rising edge. In the case of the Ni divacancy, the agreement is much better, most of the main features measured in the experiment are also present in the simulation with relatively well-matched intensities (Fig. 9). In the higher energy part some extra damping reveals probably a slightly disordered structure. In the same figure is shown ($NV_SNi_IVN_S$) the nickel divacancy with two surrounding nitrogen atoms with inversion symmetry. In both models, the atomic positions are exactly the same, the only difference being that two carbon atoms are substituted by nitrogen atoms. It can be checked that the effect of the N atoms is rather small. There is only a slight improvement for the amplitude of the pre-edge peak at 8333 eV. When using relaxed structures, the difference between both models becomes more important. This difference comes thus from the atomic displacements induced by the N atoms and not directly from its chemical nature (the photoelectron scattering effects of N and C atoms are similar). Surprisingly the nonrelaxed divacancy model (shown in the figure) is slightly better than the relaxed one. It must be said that there are different possibilities for the N sites around the Ni atoms. Some tests showed that it was not possible to discriminate among them. Most probably, these different sites are allowed and the resulting experimental spectrum is an average corresponding to the disorder evoked above. In any case, from the XANES analysis, the divacancy model is notably more likely than the other configurations.

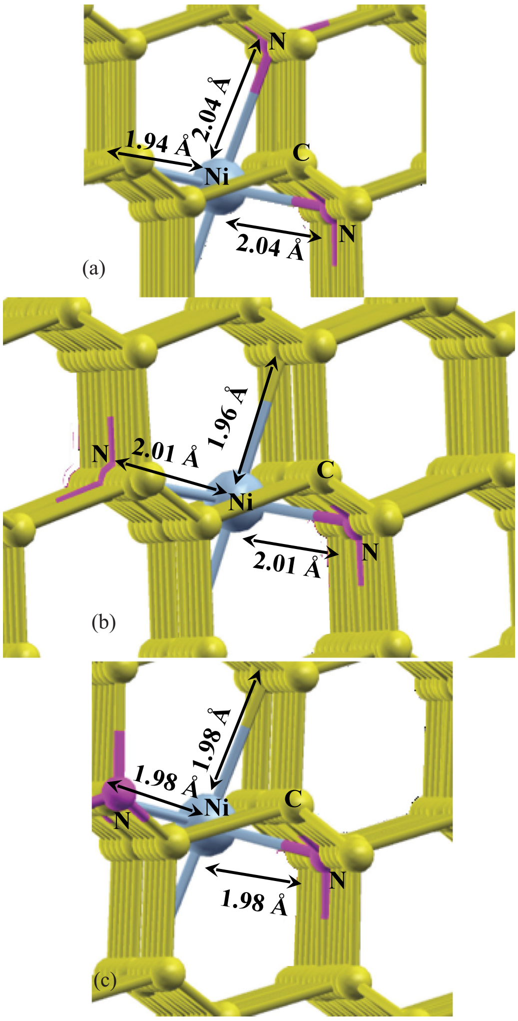

FIG. 7. (Color online) Relaxed structure of the three configurations of the Ni divacancy decorated with two substitutional nitrogen atoms: (a) ($VNi_IVN_SN_S$) two N atoms on the same side of the Ni atom, (b) ($N_SVNi_IVN_S$) one N atom on each side of the Ni atom with inversion symmetry, and (c) ($N_SVNi_IVN_S$) one N atom on each side of the Ni atom without inversion symmetry.

VI. DISCUSSION

We have searched for the most stable structures for isolated nickel, Ni-N, and Ni vacancy complexes. The formation energy calculation confirms Ni_S as a more stable state compared to Ni_I, consistently with previous studies.[28,30] More interestingly, it shows that a nickel pair Ni_SNi_S yields a 2.7 eV lower energy than two separated Ni_S atoms, suggesting a tendency for

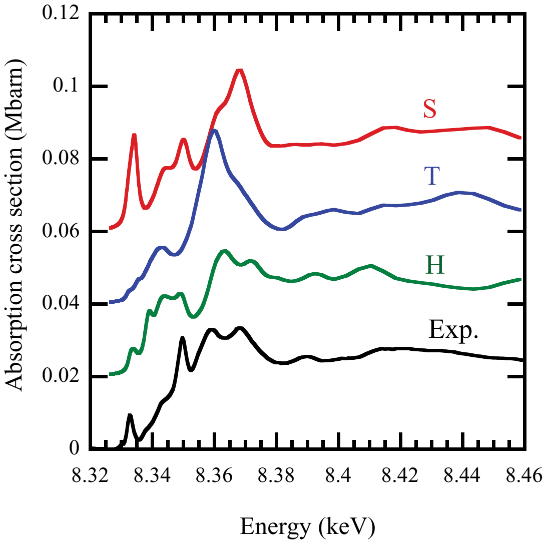

FIG. 8. (Color online) Experimental XANES and FDMNES simulated XANES spectra for substitutional Ni_S and interstitial Ni_I sites, H corresponds to the hexagonal site and T to the tetrahedral one. Spectra have been shifted vertically for clarity. Atomic positions used for the simulations are the relaxed ones.

cluster formations. In the sample studied, however, magnetic measurement indicates no ferromagnetic behavior associated with nickel clusters, but a clear paramagnetic signature related to isolated, noninteracting magnetic sites. The formation of nickel clusters was therefore prevented either by growth kinetics or by the incorporation of isolated nickel in a configuration even more energetically favorable than the cluster. With the nickel divacancy having a total energy 1.7 eV lower than that of the substitutional Ni_S, it is the most favorable configuration. Total energies cannot be compared directly because of different chemical compositions, but a diamond crystal containing two isolated Ni_S atoms will gain 2.7 eV when forming a nickel pair and 3.4 eV when forming two isolated divacancies. Thus, the calculations suggest that nickel is more favorably incorporated on divacancy sites in diamond.

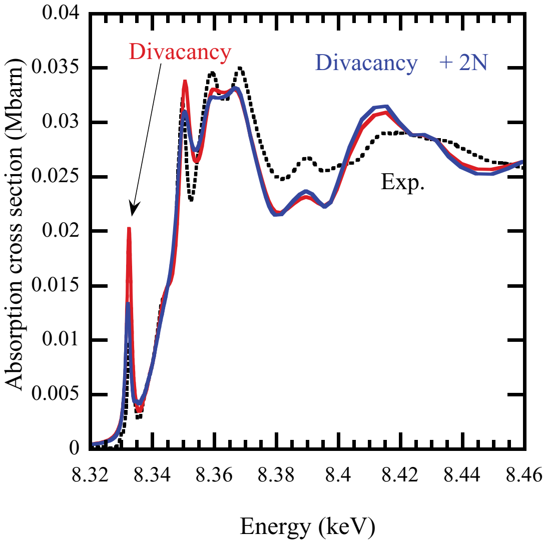

FIG. 9. (Color online) Experimental XANES and FDMNES simulated XANES spectra for Ni divacancy lattice sites. Model with and without N atoms are shown. They are very similar. The divacancy model is better than the substitutional Ni_S and interstitial Ni_I site models. Atom positions are not relaxed.

From an experimental point of view, the XANES spectrum combined with FDMNES simulations shows clearly that nickel was not incorporated in either the substitutional site or the interstitial site. The only agreement between this experiment and the simulations is obtained for the nickel-divacancy complex. Minor variations are observed on the simulated spectra depending on the number and positions of nitrogen atoms decorating the divacancy, but no clear conclusion can be drawn. Most probably the sample contains a mixture of divacancies decorated with zero to four nitrogen atoms.

These results should be compared with those of magneto-optical studies of the same crystal at low temperature and high field,[39] which showed that the Ni main luminescence line at 1.4 eV had its trigonal axis along the [111] direction in the (111) growth sectors and was distributed among the four equivalent [111] directions in the (100) growth sectors. According to a recent study,[30] the only Ni-divacancy complexes with a trigonal symmetry are those which are not decorated with any nitrogen atom, and this only in the neutral or −2 charge and 1/2 spin states. Although a general picture where Ni is incorporated on divacancy sites would seem compatible with the features of this 1.4-eV line, a more detailed study of the effect of nitrogen on the electronic structure and charge state of such a defect is necessary before making a more affirmative assignment. Complementary measurements on the same crystal such as x-ray circular magnetic dichroism (XCMD) on the Ni $L_{2,3}$ edge could provide information on the magnetic moment of the divacancy centers.

VII. CONCLUSION

The present work reports a theoretical and experimental investigation of Ni and related defects in diamond. DFT calculations were performed for different possible structures and computed results are compared to the XANES results. Theoretical calculations and experimental investigations suggest that a divacancy lattice site is most stable for nickel in the studied diamond crystal.

ACKNOWLEDGMENTS

We thankfully acknowledge P. Gaikwad (ENS Cachan) for help during the experiment at the ESRF. A.K. is thankful to the Agence Nationale pour la Recherche (Grant No. ANR 06 BLAN 0339-02), France, for providing financial support during this research. We are also thankful to J. F Roch and F. Treussart (LPQM, ENS Cachan) for fruitful discussions. The XCRYSDEN program was used to plot the relaxed atomic positions.[52]

[*] Etienne.Gheeraert@grenoble.cnrs.fr

[†] Present address: Institute for Experimental and Applied Physics, University of Regensburg, D-93040 Regensburg, Germany.

[‡] Present address: Tsukuba Expo Center, Japan.

[1] A. Gruber, A. Drabenstedt, C. Tietz, L. Fleury, J. Wrachtrup, and C. von Borczyskowski, Science **276**, 2012 (1997).

[2] A. Lohrmann, S. Pezzagna, I. Dobrinets, P. Spinicelli, V. Jacques, J. F. Roch, J. Meijer, and A. M. Zaitsev, Appl. Phys. Lett. **99**, 251106 (2011).

[3] J. R. Maze, P. L. Stanwix, J. S. Hodges, S. Hong, J. M. Taylor, P. Cappellaro, L. Jiang, M. V. G. Dutt, E. Togan, A. S. Zibrov, A. Yacoby, R. L. Walsworth, and M. D. Lukin, Nature (London) **455**, 644 (2008).

[4] G. Balasubramanian, I. Y. Chan, R. Kolesov, M. Al-Hmoud, J. Tisler, C. Shin, C. Kim, A. Wojcik, P. R. Hemmer, A. Krueger, T. Hanke, A. Leitenstorfer, R. Bratschitsch, F. Jelezko, and J. Wachtrup, Nature (London) **455**, 648 (2008).

[5] C. D. Clark, H. Kanda, I. Kiflawi, and G. Sittas, Phys. Rev. B **51**, 16681 (1995).

[6] Chunglang Wang, C. Kurtsiefer, H. Weinfurter, and B. Burchard, J. Phys. B **39**, 37 (2006); U. F. S. D'Haenens-Johansson, A. M. Edmonds, B. L. Green, M. E. Newton, G. Davies, P. M. Martineau, R. U. A. Khan, and D. J. Twitchen, Phys. Rev. B **84**, 245208 (2011).

[7] A. Collins and P. Spear, J. Phys. D Appl. Phys. **15**, L183 (1982).

[8] S. Lawson, H. Kanda, K. Watanabe, I. Kiflawi, Y. Sato, and A. Collins, J. App. Phys. **79**, 4348 (1996).

[9] A. M. Zaitsev, Phys. Rev. B **61**, 12909 (2000).

[10] T. Gaebel, I. Popa, A. Gruber, M. Domhan, F. Jelezko, and J. Wrachtrup, New J. Phys. **6**, 98 (2004).

[11] E. Wu, V. Jacques, F. Treussart, H. Zeng, P. Grangier, and J.-F. Roch, J. Lumin. **119**, 19 (2006).

[12] I. Aharonovich, C. Zhou, A. Stacey, J. Orwa, S. Castelletto, D. Simpson, A. D. Greentree, F. Treussart, J.-F. Roch, and S. Prawer, Phys. Rev. B **79**, 235316 (2009).

[13] S. Pezzagna, D. Rogalla, and D. Wildanger, New J. Phys. **13**, 035024 (2011).

[14] M. Wolfer, A. Kriele, O. A. Williams, H. Obloh, C. C. Leancu, and C. E. Nebel, Phys. Status Solidi A **206**, 2012 (2009).

[15] T. Dietl, H. Ohno, and F. Matsukura, Phys. Rev. B **63**, 195205 (2001).

[16] S. C. Erwin and C. S. Hellberg, Phys. Rev. B **68**, 245206 (2003).

[17] E. B. Lombardi, Diamond Relat. Mater. **17**, 1345 (2008).

[18] J. Rabeau, Y. Chin, S. Prawer, F. Jelezko, T. Gaebel, and J. Wrachtrup, Appl. Phys. Lett. **86**, 131926 (2005).

[19] M. Benabdesselam, P. Iacconi, D. Briand, A. Berkane-Krachai, E. Gheeraert, and H. Kanda, J. Appl. Phys. **88**, 4648 (2000).

[20] M. Benabdesselam, P. Iacconi, E. Gheeraert, H. Kanda, D. Lapraz, and D. Briand, Radiat. Prot. Dosim. **100**, 329 (2002).

[21] J. Maes, K. Iakoubovskii, M. Hayne, A. Stetsmans, and V. M. Moshchalkov, J. Phys. D: Appl. Phys. **37**, 1102 (2004).

[22] L. Paslovsky and J. E. Lowther, J. Phys. Chem. Solids **54**, 243 (1993).

[23] Y. Jinlong, Z. Manhong, and W. Kelin, Phys. Rev. B **49**, 15525 (1994).

[24] J. E. Lowther, Phys. Rev. B **51**, 91 (1995).

[25] J. Goss, A. Resende, R. Jones, S. Öberg, and P. R. Briddon, Mater. Sci. Forum **196**, 67 (1995).

[26] K. Johnston and A. Mainwood, Diamond Relat. Mater. **11**, 631 (2003).

[27] M. Watkins and A. Mainwood, J. Phys.: Condens. Matter **15**, S2913 (2004).

[28] J. P. Goss, P. R. Briddon, R. Jones, and S. Öberg, J. Phys.: Condens. Matter **16**, 4567 (2004).

[29] R. Larico, L. V. C. Assali, W. V. M. Machado, and J. F. Justo, Appl. Phys. Lett. **84**, 720 (2004); **85**, 6293 (2004).

[30] R. Larico, J. F. Justo, W. V. M. Machado, and L. V. C. Assali, Phys. Rev. B **79**, 115202 (2009).

[31] J. Isoya, H. Kanda, J. R. Norris, J. Tang, and M. K. Bowman, Phys. Rev. B **41**, 3905 (1990).

[32] J. Isoya, H. Kanda, and Y. Uchida, Phys. Rev. B **42**, 9843 (1990).

[33] V. A. Nadolinny, A. P. Yelisseyev, J. M. Baker, M. E. Newton, D. J. Twitchen, S. C. Lawson, O. P. Yuryeva, and B. N. Feigelson, J. Phys.: Condens. Matter **11**, 7357 (1999).

[34] K. Iakoubovskii, A. Stesmans, B. Nouwen, and G. J. Adriaenssens, Phys. Rev. B **62**, 16587 (2000).

[35] J. M. Baker, J. Phys.: Condens. Matter **15**, S2929 (2003).

[36] K. Iakoubovskii, Phys. Rev. B **70**, 205211 (2004).

[37] M. H. Nazaré, A. J. Neves, and G. Davies, Phys. Rev. B **43**, 14196 (1991).

[38] P. W. Mason, F. S. Ham, and G. D. Watkins, Phys. Rev. B **60**, 5417 (1999).

[39] P. Plochocka, O. Portugall, P. Y. Solane, E. Gheeraert, L. Ranno, E. Bustarret, N. Bruyant, I. Breslavetz, D. K. Maude, H. Kanda, and G. L. J. A Rikken, Phys. Rev. B **86**, 045203 (2012).

[40] G. Kresse and J. Hafner, Phys. Rev. B **47**, 558 (1993).

[41] J. P. Perdew and Y. Wang, Phys. Rev. B **33**, 8800 (1986).

[42] G. Kresse and J. Hafner, J. Phys.: Condens. Matter **6**, 8245 (1994).

[43] H. J. Monkhorst and J. D. Pack, Phys. Rev. B **13**, 5188 (1976).

[44] D. Saada, J. Adler, and R. Kalish, Phys. Rev. B **61**, 10711 (2000).

[45] J. P. Goss, R. Jones, M. I. Heggie, C. P. Ewels, P. R. Briddon, and S. Öberg, Phys. Rev. B **65**, 115207 (2002).

[46] Y. Joly, Phys. Rev. B **63**, 125120 (2001).

[47] G. Davies, A. J. Neves, and M. H. Nazaré, Europhys. Lett. **9**, 47 (1989).

[48] A. T. Collins, H. Kanda, J. Isoya, C. A. J. Ammerlaan, and J. A. van Wyk, Diamond Relat. Mater. **7**, 333 (1998).

[49] S. C. Lawson and H. Kanda, Diamond Relat. Mater. **2**, 130 (1993).

[50] J. P. Goss, R. Jones, S. J. Breuer, P. R. Briddon, and S. Öberg, Phys. Rev. Lett. **77**, 3041 (1996).

[51] D. J. Twitchen, J. M. Baker, M. E. Newton, and K. Johnston, Phys. Rev. B **61**, 9 (2000).

[52] A. Kokalj, Comput. Mater. Sci. **28**, 155 (2003).